

Modeling and analysis of common-mode current propagation in broadband power-line communication networks

Kamarul, A.; Pang, Teng Seng; So, Ping Lam; See, Kye Yak

2008

Pang, T. S., So, P. L., See, K. Y., & Kamarul, A. (2008). Modeling and analysis of common-mode current propagation in broadband power-line communication networks. IEEE Transactions on Power Delivery. 23(1), 171-179.

<https://hdl.handle.net/10356/93456>

<https://doi.org/10.1109/TPWRD.2007.911015>

© 2008 IEEE. Personal use of this material is permitted. However, permission to reprint/republish this material for advertising or promotional purposes or for creating new collective works for resale or redistribution to servers or lists, or to reuse any copyrighted component of this work in other works must be obtained from the IEEE. This material is presented to ensure timely dissemination of scholarly and technical work. Copyright and all rights therein are retained by authors or by other copyright holders. All persons copying this information are expected to adhere to the terms and constraints invoked by each author's copyright. In most cases, these works may not be reposted without the explicit permission of the copyright holder. <http://www.ieee.org/portal/site> This material is presented to ensure timely dissemination of scholarly and technical work. Copyright and all rights therein are retained by authors or by other copyright holders. All persons copying this information are expected to adhere to the terms and constraints invoked by each author's copyright. In most cases, these works may not be reposted without the explicit permission of the copyright holder.

Modeling and Analysis of Common-Mode Current Propagation in Broadband Power-Line Communication Networks

T. S. Pang, P. L. So, *Senior Member, IEEE*, K. Y. See, *Senior Member, IEEE*, and A. Kamarul

Abstract—This paper proposes a new approach to modeling the common-mode (CM) current propagation path of electrical power-line cables for broadband power-line communications (PLC). In this approach, a CM current propagation model for a three-wire power-line cable is developed using the multiconductor transmission-line theory. The model is used to study the electromagnetic-interference radiation mechanism from the PLC network in the frequency range of 1 to 30 MHz. The accuracy of the model is verified through numerical simulations and practical measurements conducted on the actual power-line network. The developed model allows us to predict the CM current in the power-line cable with reasonable accuracy.

Index Terms—Common-mode current propagation model, electromagnetic-interference (EMI) analysis, power-line communications (PLC).

I. INTRODUCTION

POWER-LINE communications (PLC) is a term used to identify technologies, equipment, applications, and services that allow users to communicate over existing power lines. The most attractive advantage of this technology is that the power-line network is the most pervasive and accessible network that reaches every power socket in every home. Since the power-line network is already installed, there is no need to lay new cables. Efforts to use this technology began as early as in the 1830s [1], when narrowband applications were developed; however, they were restricted to power-line signaling electricity meters. It was only in the 1990s that the idea of using the residential power grid to offer value-added digital communication services became more popular due to the development of the HomePlug Powerline Alliance [2]. The HomePlug Powerline Alliance is an industry-led initiative to establish standards for PLC companies. It has established specifications heading for data rates as high as 200 Mb/s [2].

Although PLC technology has the advantage of requiring “no new wires,” the major obstacle to its widespread use in broadband communication is the risk of electromagnetic interference (EMI). The power-line cables in use are designed to carry electrical power, not radio signals. The broadband PLC signals have a frequency bandwidth of 1–30 MHz. Since the power-line cables are not shielded, they behave like long antennas when high-

Manuscript received December 14, 2006; revised April 19, 2007. This work was supported by the Nanyang Technological University of Singapore. Paper no. TPWRD-00801-2006.

The authors are with the PLC Research Group, Network Technology Research Center, School of Electrical and Electronic Engineering, Nanyang Technological University, Singapore 639798 (e-mail: eplso@ntu.edu.sg).

Digital Object Identifier 10.1109/TPWRD.2007.911015

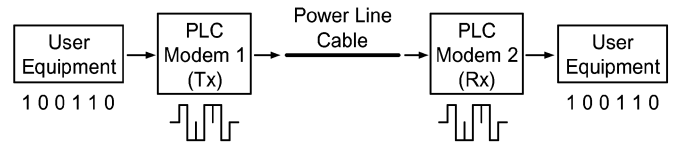


Fig. 1. Data communication between two PLC modems over a power-line cable.

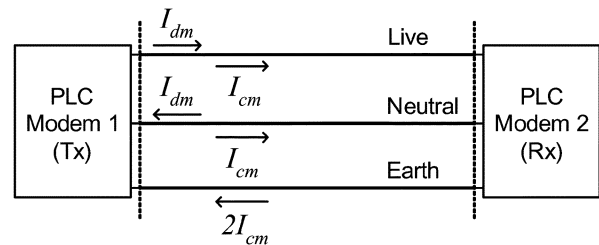


Fig. 2. CM current propagation paths in a PLC system.

frequency PLC signals are transmitted. This can cause EMI for services operating in the same frequency range. The high levels of emitted radiation [3], [4] are a concern for many international regulatory bodies. Further, the frequency bands of 1–30 MHz are the same as those used for broadcasting, military communications, aeronautical/maritime safety services, radio amateurs, and others. As long as the EMI issue is not resolved, there would be a major concern for the widespread deployment of broadband PLC technology [5], [6].

There are two forms of electromagnetic disturbances, namely: 1) differential-mode (DM) and 2) common-mode (CM) signals [7]. DM signals are also known as symmetrical mode signals or transverse signals, while CM signals are also called asymmetrical mode signals or longitudinal signals. Since DM currents flow in the opposite direction, the electromagnetic fields generated by the currents actually cancel out each other and are not so much of an EMI concern. However, CM currents flow in the same direction, causing the electromagnetic fields to add up. This results in significant levels of EMI radiation, even if only a low level of CM current is flowing. In a PLC system, DM currents are the signals required for transmission, whereas CM currents are the undesired signals that are generated due to the unbalance of the power-line cable which converts a portion of the transmitted DM signals into CM signals [8]. Since the CM currents are the main cause of electromagnetic radiation from the PLC network, it is necessary to study the characteristics of the propagation of CM currents in the PLC network.

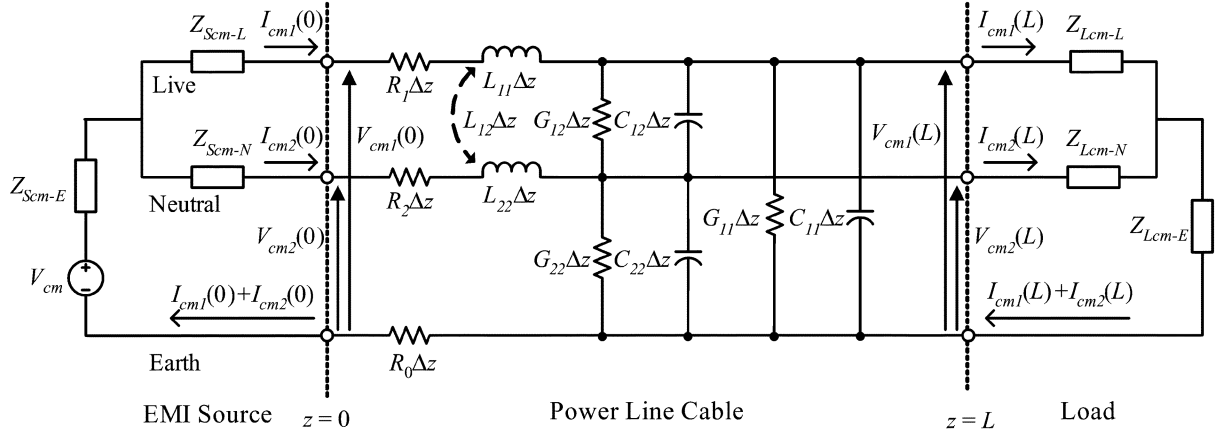


Fig. 3. Three-wire equivalent CM current propagation model of a power-line cable.

In this paper, a CM current propagation model for a three-wire power-line cable is derived using the multiconductor transmission-line (MTL) theory. The model is used to characterize and understand the behavior of CM currents in the PLC network. The developed model allows us to predict the CM currents in the PLC network with reasonable accuracy. With this knowledge, we can better understand the EMI radiation mechanism from the PLC network and this will help us to explore new injection techniques to suppress radiated emissions from the PLC network.

II. CM CURRENT PROPAGATION MODEL

Fig. 1 shows a simple PLC system which consists of a computer connected to one PLC modem at one end of the power-line cable and another computer connected to another PLC modem at the other end. Communication signals are converted from digital to analog in the PLC modem and transmitted through the power-line cable. At the receiving end, the PLC modem converts the analog signals back into digital form.

The signal propagation paths in the PLC system are shown in Fig. 2. In this model, we have a three-wire power-line cable in which the Earth wire is the reference conductor. The DM current I_{dm} flows in the Live wire from PLC modem 1 to PLC modem 2 and returns via the Neutral wire. The CM currents I_{cm} flow from PLC modem 1 to PLC modem 2 in the Live and Neutral wires and return to PLC modem 1 via the Earth wire.

The three-wire equivalent CM current propagation model is shown in Fig. 3, with PLC modem 1 as the CM noise source and PLC modem 2 as the load. The CM noise source consists of the CM source voltage V_{cm} and CM source impedances Z_{Scm-L} , Z_{Scm-N} and Z_{Scm-E} . PLC modem 2 is represented by its own internal CM impedances Z_{Lcm-L} , Z_{Lcm-N} , and Z_{Lcm-E} , which act as the CM terminating load. R_0 , R_1 , and R_2 are the effective CM resistances per unit length (in ohms per meter); G_{11} , G_{12} , and G_{22} are the effective CM conductances per unit length (in Siemens (S) per meter); L_{11} , L_{12} , and L_{22} are the effective CM inductances per unit length (in Henries (H) per meter); C_{11} , C_{12} , and C_{22} are the effective CM capacitances per unit length (in Farads (F) per meter). All of the aforementioned parameters can be derived from the properties of the cable.

The effective per-unit-length CM resistance matrix, CM conductance matrix, CM inductance matrix, and CM capacitance matrix are as follows:

$$R = \begin{bmatrix} R_0 + R_1 & R_0 \\ R_0 & R_0 + R_2 \end{bmatrix} \quad (1)$$

$$G = \begin{bmatrix} G_{11} + G_{12} & -G_{12} \\ -G_{12} & G_{12} + G_{22} \end{bmatrix} \quad (2)$$

$$L = \begin{bmatrix} L_{11} & L_{12} \\ L_{12} & L_{22} \end{bmatrix} \quad (3)$$

$$C = \begin{bmatrix} C_{11} + C_{12} & -C_{12} \\ -C_{12} & C_{12} + C_{22} \end{bmatrix}. \quad (4)$$

With knowledge of these matrices, we can compute the Z and Y matrices which are the per-unit-length impedance and admittance matrices, respectively

$$Z = R + j\omega L \quad (5)$$

$$Y = G + j\omega C. \quad (6)$$

Since the matrices obtained are symmetrical, we take the transformation matrix T as follows [9]:

$$T = \frac{1}{\sqrt{2}} \begin{bmatrix} 1 & 1 \\ 1 & -1 \end{bmatrix}. \quad (7)$$

A diagonal matrix γ^2 is computed using the T , Y , and Z matrices

$$\gamma^2 = T^{-1} Y Z T = \begin{bmatrix} \gamma_1^2 & 0 & \cdots & 0 \\ 0 & \gamma_2^2 & \ddots & \vdots \\ \vdots & \ddots & \ddots & 0 \\ 0 & \cdots & 0 & \gamma_n^2 \end{bmatrix}. \quad (8)$$

The characteristic impedance matrix Z_0 can be calculated as

$$Z_0 = Y^{-1} T \gamma T^{-1} = Z T \gamma^{-1} T^{-1} \quad (9)$$

and $\sqrt{Y Z}$ can be derived as

$$\sqrt{Y Z} = T \gamma T^{-1}. \quad (10)$$

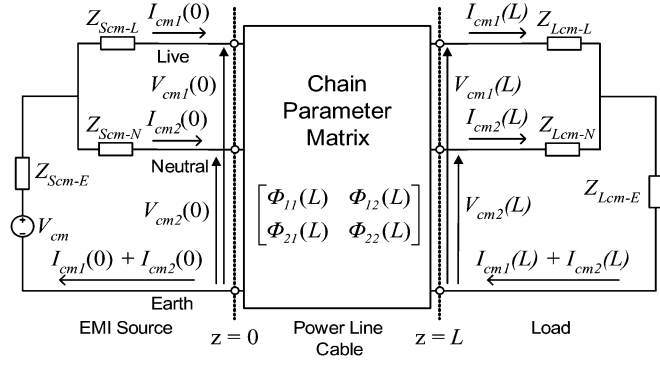


Fig. 4. CM noise propagation model using the chain parameter matrix.

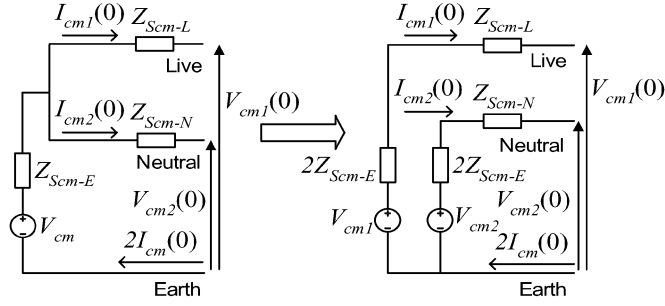


Fig. 5. Modeling of the source termination of the power-line cable.

The chain parameter matrix can be computed as

$$\Phi_{11}(L) = \cosh(\sqrt{ZY}L) = Y^{-1} \cosh(\sqrt{YZ}L)Y \quad (11)$$

$$\Phi_{12}(L) = -Z_0 \sinh(\sqrt{YZ}L) = -\sinh(\sqrt{ZY}L)Z_0 \quad (12)$$

$$\Phi_{21}(L) = -Z_0^{-1} \sinh(\sqrt{ZY}L) = -\sinh(\sqrt{YZ}L)Z_0^{-1} \quad (13)$$

$$\Phi_{22}(L) = \cosh(\sqrt{YZ}L) = Y \cosh(\sqrt{ZY}L)Y^{-1}. \quad (14)$$

The three-wire equivalent CM noise propagation model of the power-line cable in Fig. 3 can be represented by its chain parameter matrix as shown in Fig. 4. The source termination and the load termination of the power-line cable are represented in Figs. 5 and 6, respectively. In Fig. 5, the CM source voltage V_{cm} can be seen as two separate sources V_{cm1} and V_{cm2} , supplying CM voltages to the Live and Neutral wires, respectively (i.e., $V_{cm} = V_{cm1} = V_{cm2}$). Since the CM currents flowing in the Live and Neutral wires are equal, $I_{cm1}(0) = I_{cm2}(0) = I_{cm}(0)$, where $I_{cm}(0)$ is half of the CM current flowing in the Earth wire. By decoupling the CM source voltage V_{cm} into two separate sources (V_{cm1} and V_{cm2}), each CM voltage source (V_{cm1} and V_{cm2}) sees a CM source impedance of $2Z_{Scm-E}$ as the current flowing through that branch is only $I_{cm}(0)$ instead of $2I_{cm}(0)$. The same analysis is applied to the load termination of the power-line cable in Fig. 6.

The relationship between the injected CM voltage and the CM current at the source and that at any point on the transmission line is given by the chain parameter matrix as follows:

$$\begin{bmatrix} V(L) \\ I(L) \end{bmatrix} = \Phi(L) \begin{bmatrix} V(0) \\ I(0) \end{bmatrix} \quad (15)$$

where L is the length of the power-line cable.

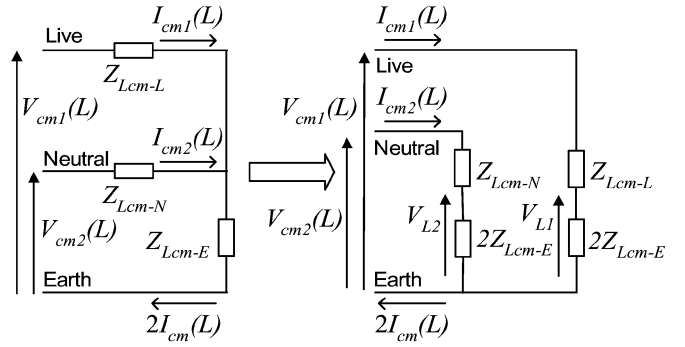


Fig. 6. Modeling of the load termination of the power-line cable.

The generalized Thevenin equivalent representations at the terminals relating the voltages and the currents are as follows:

$$V(0) = V_S - Z_S I(0) \quad (16)$$

$$V(L) = V_L + Z_L I(L) \quad (17)$$

where

$$V(0) = \begin{bmatrix} V_{cm1}(0) \\ V_{cm2}(0) \end{bmatrix}, \quad V_S = \begin{bmatrix} V_{cm1} \\ V_{cm2} \end{bmatrix} = \begin{bmatrix} V_{cm} \\ V_{cm} \end{bmatrix},$$

$$Z_S = \begin{bmatrix} 2Z_{Scm-E} + Z_{Scm-L} & 0 \\ 0 & 2Z_{Scm-E} + Z_{Scm-N} \end{bmatrix},$$

$$I(0) = \begin{bmatrix} I_{cm1}(0) \\ I_{cm2}(0) \end{bmatrix} = \begin{bmatrix} I_{cm}(0) \\ I_{cm}(0) \end{bmatrix}, \quad V(L) = \begin{bmatrix} V_{cm1}(L) \\ V_{cm2}(L) \end{bmatrix},$$

$$V_L = \begin{bmatrix} V_{L1} \\ V_{L2} \end{bmatrix} = \begin{bmatrix} I_{cm1}(L) \cdot 2Z_{Lcm-E} \\ I_{cm2}(L) \cdot 2Z_{Lcm-E} \end{bmatrix},$$

$$Z_L = \begin{bmatrix} Z_{Lcm-L} & 0 \\ 0 & Z_{Lcm-N} \end{bmatrix} \quad \text{and}$$

$$I(L) = \begin{bmatrix} I_{cm1}(L) \\ I_{cm2}(L) \end{bmatrix} = \begin{bmatrix} I_{cm}(L) \\ I_{cm}(L) \end{bmatrix}.$$

III. DETERMINATION OF LINE PARAMETERS

In order to obtain the chain parameter matrix, we need to first derive the per-unit-length matrices of the power-line cable based on its properties.

A. Resistance

Skin effect is the phenomenon where more current flows near the outer surface of the wire instead of toward the center of the wire when an alternating current flows in the wire. This effect causes an increase in the effective resistance of the wire when the frequency of the current increases. In calculating this resistance, we assume that the current flows only within the skin depth of the wire. The skin depth δ is given by [9]

$$\delta = \frac{1}{\sqrt{\pi f \mu \sigma}} \quad (18)$$

where μ is the permeability of the metal wire and σ is the conductivity of the metal wire. The high frequency per-unit-length CM resistance for a wire of radius r_w in a homogeneous medium can be approximated by

$$R_w = \frac{1}{2\pi r_w \sigma \delta}. \quad (19)$$

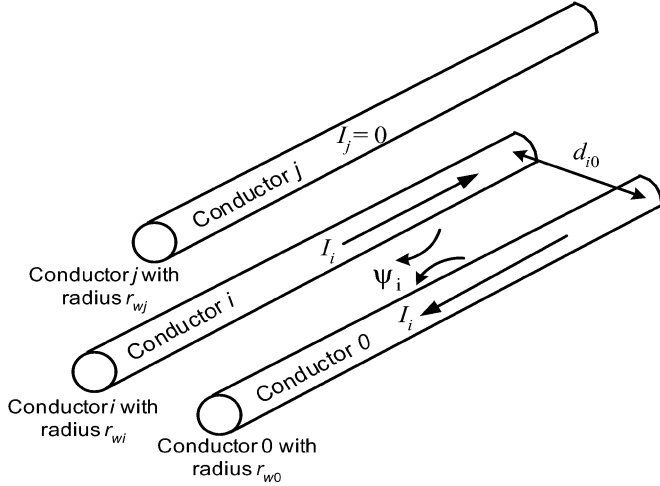


Fig. 7. Illustration of the calculation of per-unit-length self-inductance.

Since the wires are all identical, the per-unit-length CM resistance matrix is obtained as

$$R = \begin{bmatrix} 2R_w & R_w \\ R_w & 2R_w \end{bmatrix}. \quad (20)$$

B. Inductance

To derive the per-unit-length CM inductance and capacitance matrices of the power-line cable, knowledge of the static electromagnetic analysis is required. Basically, the inductance is determined based on the principle of magnetostatics. Deriving the inductances for the power-line cable requires consideration of the magnetic flux ψ_i that penetrates a surface that is parallel to the cable when a current flows [9].

Consider the case of three wires in a homogeneous medium. The self-inductance is obtained from Fig. 7 by considering the total magnetic flux ψ_i that penetrates the surface parallel to conductor i and conductor 0 when there is no current flowing in conductor j and a current I_i flows in conductor i and returns through conductor 0. This gives us self-inductance L_{ii} [9] as

$$\begin{aligned} L_{ii} &= \frac{\psi_i}{I_i} \Big|_{I_j=0} \\ &= \frac{\mu}{2\pi} \ln \left(\frac{d_{i0}}{r_{wi}} \right) + \frac{\mu}{2\pi} \ln \left(\frac{d_{i0}}{r_{w0}} \right) \\ &= \frac{\mu}{2\pi} \ln \left(\frac{d_{i0}^2}{r_{wi}r_{w0}} \right). \end{aligned} \quad (21)$$

The mutual inductance is obtained from Fig. 8 by considering the total magnetic flux ψ_i that penetrates the surface parallel to conductor i and conductor 0 when there is no current flowing in conductor i and a current I_j flows in conductor j and returns through conductor 0. This gives us the mutual inductance L_{ij} [9] as

$$\begin{aligned} L_{ij} &= \frac{\psi_i}{I_j} \Big|_{I_i=0} \\ &= \frac{\mu}{2\pi} \ln \left(\frac{d_{j0}}{d_{ij}} \right) + \frac{\mu}{2\pi} \ln \left(\frac{d_{i0}}{r_{w0}} \right) \\ &= \frac{\mu}{2\pi} \ln \left(\frac{d_{i0}d_{j0}}{d_{ij}r_{w0}} \right). \end{aligned} \quad (22)$$

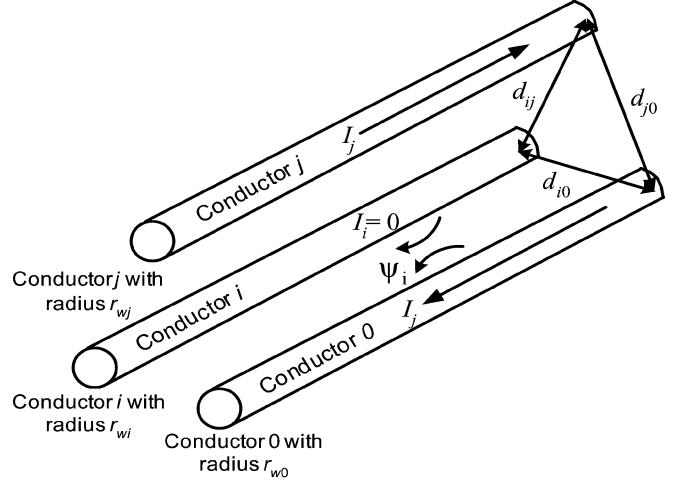


Fig. 8. Illustration of the calculation of per-unit-length mutual inductance.

However, again the skin effects need to be considered. The skin effects not only cause an increase in wire resistance but also cause a decrease in self-inductance. According to [10], the self-inductance for conductor i can be corrected by multiplying it by a correction factor of

$$X_i = \frac{1}{0.315 \times 0.53 \times \frac{r_{wi}}{\delta}} \quad (23)$$

where r_{wi} is the radius of conductor i .

The corrected self-inductance is finally obtained as

$$L_{ii \text{ corr}} = X_i \cdot \frac{\mu}{2\pi} \ln \left(\frac{d_{i0}}{r_{wi}} \right) + X_0 \cdot \frac{\mu}{2\pi} \ln \left(\frac{d_{i0}}{r_{w0}} \right) \quad (24)$$

where X_i is the correction factor for the conductor i and X_0 is the correction factor for the conductor 0.

The mutual inductance also needs to be corrected in order to take into account the skin effects. The corrected mutual inductance is finally obtained as

$$L_{ij \text{ corr}} = X_j \cdot \frac{\mu}{2\pi} \ln \left(\frac{d_{j0}}{d_{ij}} \right) + X_0 \cdot \frac{\mu}{2\pi} \ln \left(\frac{d_{i0}}{r_{w0}} \right) \quad (25)$$

where X_j is the correction factor for the conductor j .

The per-unit-length CM inductance matrix is finally written as

$$L = \begin{bmatrix} L_{ii \text{ corr}} & L_{ij \text{ corr}} \\ L_{ji \text{ corr}} & L_{jj \text{ corr}} \end{bmatrix}_{i=1, j=2}. \quad (26)$$

C. Capacitance

The per-unit-length CM capacitance matrix for the power-line cable is derived based on the principle of electrostatics. The equivalent coupling effects occurring inside the power-line cable are shown in Fig. 9. C_{pair} is the per-unit-length CM capacitance between any two parallel wires.

The capacitance between any two wires is given by [11]

$$C_{\text{pair}} = \frac{\pi \epsilon}{\ln \left[\left(\frac{D}{2a} \right) + \sqrt{\left(\frac{D}{2a} \right)^2 - 1} \right]} \quad (27)$$

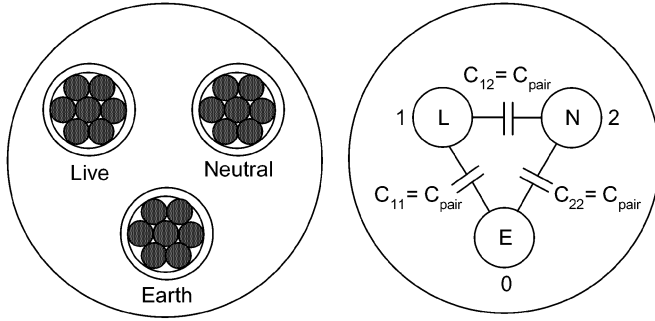


Fig. 9. Cross-sectional view of the power-line cable and the per-unit-length capacitance between any two wires.

where D is the distance between any two wires and a is the radius of the wire. The per-unit-length CM capacitance matrix is given by

$$C = \begin{bmatrix} 2C_{\text{pair}} & -C_{\text{pair}} \\ -C_{\text{pair}} & 2C_{\text{pair}} \end{bmatrix}. \quad (28)$$

D. Conductance

From [11], if the surrounding medium is homogenous, we can obtain

$$\frac{C}{G} = \frac{\varepsilon}{\sigma_d} \Rightarrow G = \frac{\sigma_d C}{\varepsilon} \quad (29)$$

where σ_d and ε are the conductivity and permittivity of the dielectric material, respectively and G is the conductance of the wire.

Since the wires of the household power cable shown in Fig. 9 are in close proximity to each other, we assume that the dielectric material is homogenous and is made up of a mixture of insulation material and air. Based on this assumption, and from (28), we obtain

$$G = \frac{\sigma_d}{\varepsilon} C = \frac{\sigma_d}{\varepsilon} \begin{bmatrix} 2C_{\text{pair}} & -C_{\text{pair}} \\ -C_{\text{pair}} & 2C_{\text{pair}} \end{bmatrix}. \quad (30)$$

IV. EXPERIMENTAL VERIFICATION

The experimental setup is shown in Fig. 10. The CM source consists of a signal generator, an isolation transformer, and two 22 nF “Y” class coupling capacitors. The power-line cable used is a single-core PVC-insulated, nonsheathed cable with a voltage rating of 450/750 V. Its specifications match those of cables commonly used in the wiring of homes. The power-line cable is 3 m in length, and each wire is made up of copper conductors that are stranded and insulated with PVC. The wire has a cross-sectional area of 2.5 mm², and the diameter of a single copper strand is 0.67 mm. The power-line cable is terminated with a line impedance stabilization network (LISN), which acts as the balanced load. The frequency range of interest is from 1 to 30 MHz. We limit the scope of the current experiments to

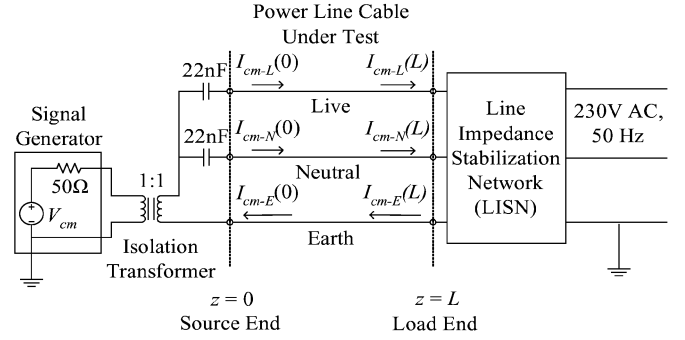


Fig. 10. Setup for the verification of the CM noise propagation model.

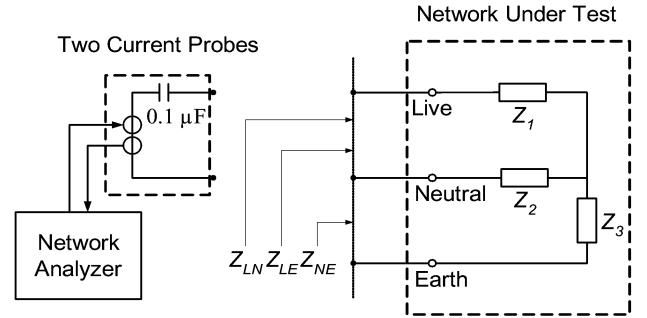


Fig. 11. Setup for the measurement of impedances using two current probes.

scenarios in which the loads are balanced, and the cables are equidistant as they run parallel to each other.

With knowledge of the properties of the power-line cable, the chain parameter matrix can be calculated. The CM current values for the Live, Neutral, and Earth wires at the source end are measured using the RF current probe. Since the CM source is known, the CM current values for the Live, Neutral and Earth wires at the load end can be derived. The derived CM current values for the Live, Neutral, and Earth wires at the load end can then be compared to those measured using the RF current probe. This comparison serves as a verification of the CM noise propagation model.

The impedances of the source and the load are measured using a two-current-probe measurement approach. The advantage of using this approach is that it allows measurement of the impedances in the presence of a high-voltage level in the power-line network without damaging the network analyzer. The details on the theory behind the two-current-probe measurement methodology can be found in [12] and will not be discussed here.

The setup for the measurement of the impedances using the two-current-probe method is shown in Fig. 11. The impedances Z_{LN} , Z_{LE} , and Z_{NE} are measured when the terminals of the two current probes are connected across the Live and Neutral wires, Live and Earth wires, and Neutral and Earth wires, respectively. From the aforementioned, we obtain

$$Z_{LN} = Z_1 + Z_2 \quad (31)$$

$$Z_{LE} = Z_1 + Z_3 \quad (32)$$

$$Z_{NE} = Z_2 + Z_3. \quad (33)$$

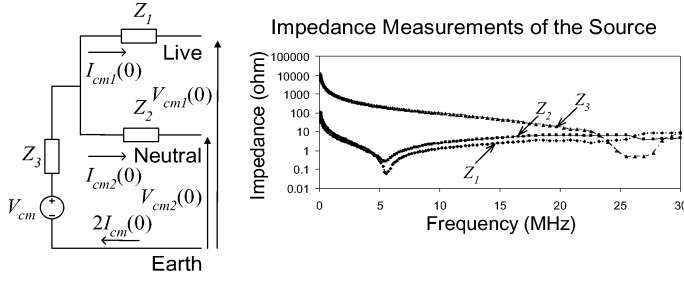


Fig. 12. Measured impedances of the source.

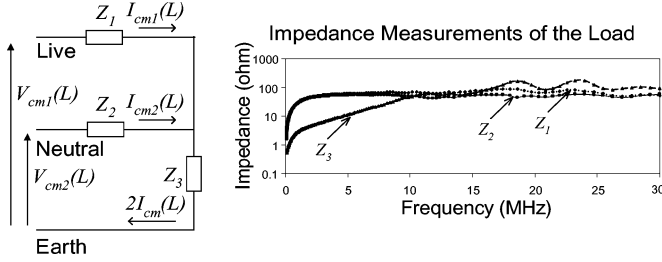


Fig. 13. Measured impedances of the load.

The relationship between the measured impedances and the network parameters Z_1 , Z_2 , and Z_3 is given by

$$Z_1 = \frac{Z_{LN} + Z_{LE} - Z_{NE}}{2} \quad (34)$$

$$Z_2 = \frac{Z_{LN} + Z_{NE} - Z_{LE}}{2} \quad (35)$$

$$Z_3 = \frac{Z_{LE} + Z_{NE} - Z_{LN}}{2} \quad (36)$$

Fig. 12 shows the measured impedances of the source which comprises a signal generator, an isolation transformer, and two 22-nF capacitors as shown in Fig. 10. In Fig. 12, Z_1 , Z_2 , and Z_3 correspond to the values of the impedances of Z_{Scm-L} , Z_{Scm-N} , Z_{Scm-E} of Fig. 5, respectively. From the figure, it can be seen that from 0 MHz to around 6 MHz, the impedances of Z_1 and Z_2 fall from a maximum value of 100 Ω to a minimum of around 0.1 Ω , and after 6 MHz, the impedances of Z_1 and Z_2 rise gradually. This is the property of a series resonant circuit with its CM capacitive impedance below the resonant frequency and its CM inductive impedance above it.

Fig. 13 shows the measured impedances of the load, with the load end being terminated with LISN. As the ac power mains has the property of varying impedance over time, the use of LISN as the terminating load provides the stabilized impedance and the repeatability of measurement results. In Fig. 13, Z_1 , Z_2 , and Z_3 correspond to the values of the impedances of Z_{Lcm-L} , Z_{Lcm-N} , Z_{Lcm-E} of Fig. 6, respectively. From Figs. 12 and 13, it can be seen that Z_1 and Z_2 in both graphs are almost equal to each other. When Z_1 is not equal to Z_2 , a portion of the injected signal is converted into CM signals [8]. Since Z_1 is equal to Z_2 at the source and load, this means that both the source and load are balanced and no additional CM signals will be generated when we inject currents into the Live and Neutral wires. This will allow us to monitor the

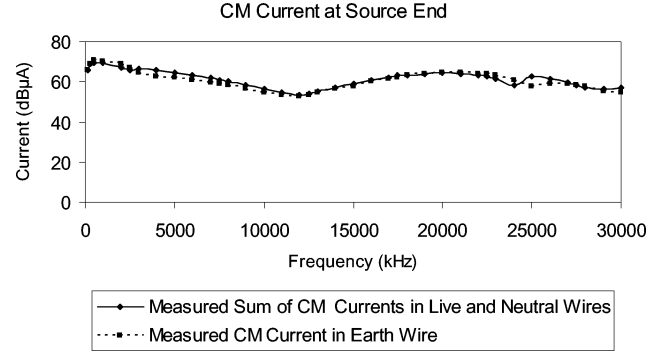


Fig. 14. Comparison of the sum of the CM currents measured in the Live and Neutral wires with the CM current measured in the Earth wire at the source end of a 3-m cable.

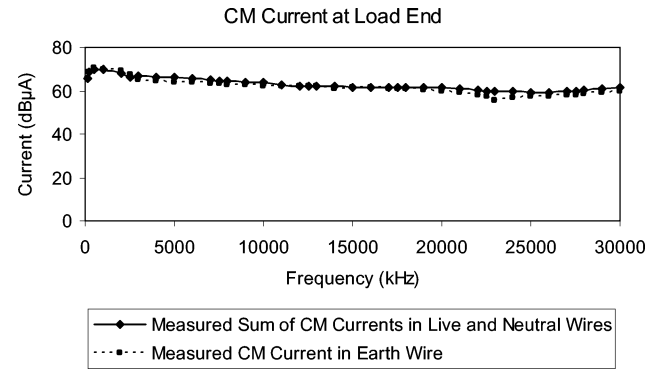


Fig. 15. Comparison of the sum of the CM currents measured in the Live and Neutral wires with the CM current measured in the Earth wire at the load end of a 3-m cable.

propagation path of the signals that we inject into the network. The value of Z_3 will not affect the symmetry of the whole network. It will only affect the level of CM current but not the level of DM current as only CM current will flow through Z_3 . This means that if we can increase Z_3 without affecting Z_1 and Z_2 , we can effectively decrease the CM current flowing through the PLC network.

In Figs. 14 and 15, the sum of the CM currents measured in the Live and Neutral wires are compared with the CM current measured in the Earth wire at both the source and load ends. The comparison shows a close agreement between the sum of the CM currents measured in the Live and Neutral wires and the CM current measured in the Earth wire. This verifies the CM current propagation model that we proposed in Fig. 2, even at high frequencies, and demonstrates that the Earth wire is the dominant return path of the CM current in a three-wire cable.

In Figs. 16 and 17, the CM currents measured in the Live and Neutral wires are compared with those of the simulated results at the source end of a 3-m power-line cable. The comparison is made based on injecting a known CM voltage of $V_{cm} = 100$ mV using a signal generator. The CM currents $I_{cm1}(0)$, $I_{cm2}(0)$, $I_{cm1}(L)$, and $I_{cm2}(L)$ are measured using a current probe (see Fig. 10). With knowledge of the measured impedance of the load from Fig. 13, the CM voltage at the load end $V_{cm1}(L)$ and $V_{cm2}(L)$ can be calculated. Knowing $V_{cm1}(L)$, $V_{cm2}(L)$, $I_{cm1}(L)$, and $I_{cm2}(L)$ at the load end, the

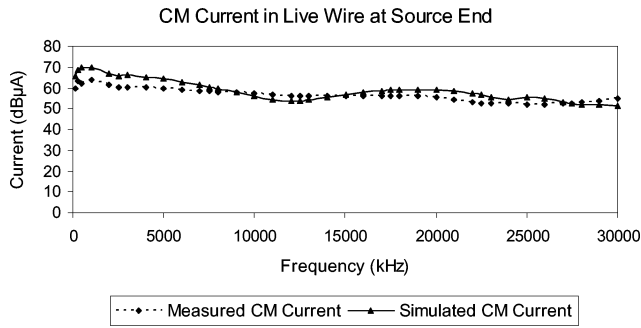


Fig. 16. Comparison of the measured and simulated CM currents in the Live wire at the source end of a 3-m cable.

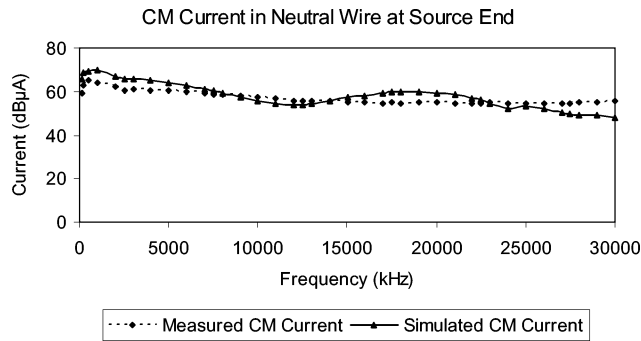


Fig. 17. Comparison of the measured and simulated CM currents in the Neutral wire at the source end of a 3-m cable.

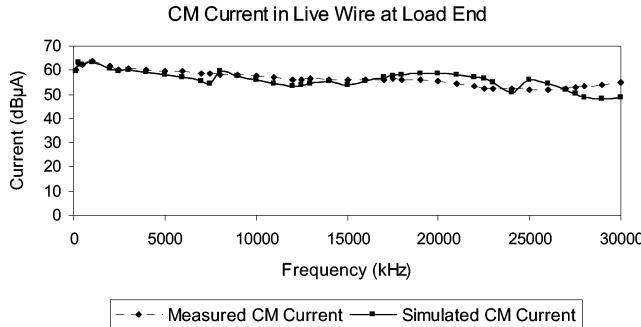


Fig. 18. Comparison of the measured and simulated CM currents in the Live wire at the load end of a 3-m cable.

CM currents $I_{cm1}(0)$ and $I_{cm2}(0)$ at the source end can be derived using (15). The calculated values are then compared with the measured values. From these figures, it can be seen that the graphs of the simulated results of the CM currents in the Live and Neutral wires at the source end are close to those of the measured results.

In Figs. 18 and 19, the CM currents measured in the Live and Neutral wires are compared with those of the simulated results at the load end of a 3-m power-line cable. Similarly, a known CM voltage of $V_{cm} = 100$ mV is injected using a signal generator. The CM currents $I_{cm1}(0)$, $I_{cm2}(0)$, $I_{cm1}(L)$, and $I_{cm2}(L)$ are measured using a current probe (see Fig. 10). With knowledge of the measured impedance of the source from Fig. 12, the CM voltage V_{cm} injected and the CM currents $I_{cm1}(0)$ and $I_{cm2}(0)$ measured, the CM voltages at the source end $V_{cm1}(0)$ and $V_{cm2}(0)$ can be calculated using the basic circuit theorem.

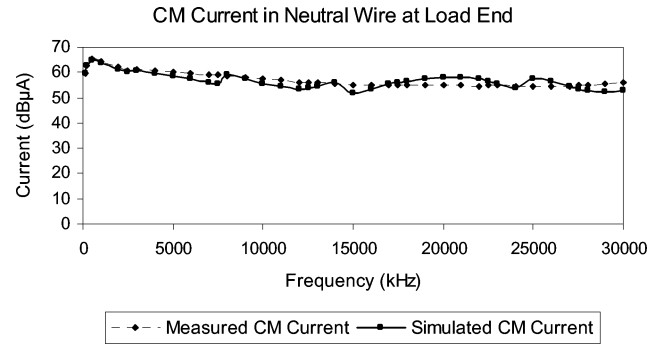


Fig. 19. Comparison of the measured and simulated CM currents in the Neutral wire at the load end of a 3-m cable.

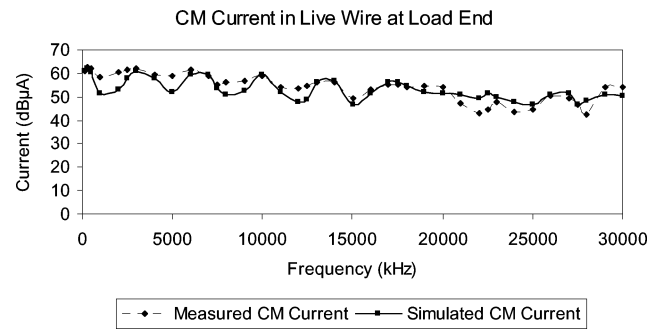


Fig. 20. Comparison of the measured and simulated CM currents in the Live wire at the load end of a 30-m cable.

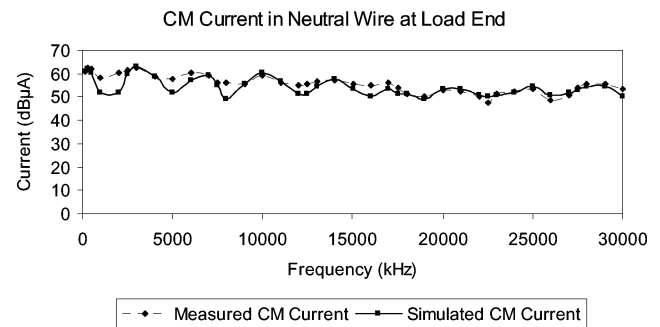


Fig. 21. Comparison of the measured and simulated CM currents in the Neutral wire at the load end of a 30-m cable.

Knowing $V_{cm1}(0)$, $V_{cm2}(0)$, $I_{cm1}(0)$ and $I_{cm2}(0)$ at the source end, the CM currents $I_{cm1}(L)$ and $I_{cm2}(L)$ are calculated at the load end using (15). The calculated values are then compared with the measured values. It can be seen from these figures that the graphs of the simulated results of the CM currents in the Live and Neutral wires at the load end correspond well with those of the measured results.

The experiment was repeated using a 30-m-long power-line cable. In Figs. 20 and 21, the CM currents measured in the Live and Neutral wires are compared with those of the simulated results at the load end of a 30-m power-line cable. From these figures, it can be seen that the graphs of the CM currents measured in the Live and Neutral wires at the load end are close to those of the simulated results for the longer cable. It is noted that there are points of maxima and minima in these graphs which are the result of the quarter-wavelength effect in

the transmission line. The quarter-wavelength effect causes such maxima or minima to occur when the cable length is equal to multiples of the quarter wavelength of the operating signal. This quarter-wavelength effect is more visible in cables of longer length than in cables of shorter length. Another observation is that there is a general downward trend in the magnitude of the CM current with increasing operating frequency. For the 3-m-long power-line cable, the magnitude of the CM currents taken at 1 MHz in both the Live and Neutral wires is around 64 dB μ A and it falls to around 53 dB μ A at 27.5 MHz as seen in Figs. 18 and 19. This downward trend is also observed in the longer 30-m-long cable where the magnitude of the CM currents measured at 1 MHz is around 63 dB μ A and the value falls to around 46 dB μ A at 27.5 MHz in Figs. 20 and 21. This downward trend clearly demonstrates that the propagated signals attenuate more at higher frequencies which is the property of wave behavior propagating through the transmission line.

The six graphs that are shown, which compare the measured CM currents with the simulated CM currents, indicate that the two currents are close to one another. From these results, we have shown that the proposed CM noise propagation model can accurately predict the CM currents at the load end for any length of power-line cable when we know the CM currents at the source end, and vice versa.

V. CONCLUSION

In this paper, a CM noise propagation model has been proposed for power-line cables based on the multiconductor transmission-line theory. The model uses a three-wire power-line cable as a realistic representation of the actual power-line network. The distributed per-unit-length CM propagation parameters of the power-line cable are derived based on the properties of the power-line cable using a bottom-up approach. Once these parameters are known, the chain parameter matrix can be derived for any length of the power-line cable and the CM noise current can then be calculated at any point of the power-line cable. With knowledge of the CM noise propagation model of the power-line cable, the level of the CM current in the power-line cable can be estimated with reasonable accuracy for different cable lengths and different loading conditions.

From the experimental results, we have seen that the dominant return path of the CM noise current is through the Earth wire of the three-wire cable. Also, the measured and simulated values of the CM noise current are compared, and it is concluded that the proposed CM noise propagation model is accurate in estimating the CM noise current at any point of the power-line cable.

We can see the experimental results from Figs. 12 and 13 that the value of Z_3 will not affect the symmetry of the whole network. It will only affect the level of the CM current. By increasing Z_3 without affecting Z_1 and Z_2 , we can effectively decrease the CM current flowing in the PLC network. Currently, our PLC research group is working on a new injection technique to increase the value of Z_3 at the injection point to reduce the CM current, and the results thus far are encouraging.

In the proposed model, we have dealt only with a system that has balanced loads. The importance of this model is that it has shown that the CM noise currents can be accurately modeled. This gives us the foundation to further understand the PLC network. With this encouraging preliminary result, we can further work with loads which are unbalanced. Also, by combining this model with a DM current propagation model, we can study the conversion of DM signals into CM signals and the impact of asymmetry of the system on the CM noise currents generated. On top of that, this model can be extended to model CM noise currents in more complicated networks, such as in tree and ring topologies. With the ability to model such complex networks, we can apply it to model the CM noise currents in a room or even in a building. Once this is achieved, we can use the model to predict the level of radiation emitted from the PLC networks.

REFERENCES

- [1] P. A. Brown, "Power line communications—Past, present and future," in *Proc. ISPLC Conf.*, 1999, pp. 1–8.
- [2] [Online]. Available: <http://www.homeplug.org>.
- [3] K. Asano, M. Shin, Y. Matsuura, K. Maegawa, S. Yamamoto, and N. Nakayama, "Experimental study of the electromagnetic radiation caused by PLC with high frequency band signals," in *Proc. ISPLC Conf.*, 2004, pp. 143–148.
- [4] C. Muto, N. Mori, and T. Kondoh, "On radio interference assessments of access PLC system," in *Proc. ISPLC Conf.*, 2003, pp. 67–72.
- [5] G. Box, BPL: The RFI Challenge [Online]. Available: http://www.arri.org/tis/info/HTML/plc/files/BPL_paper.pdf.
- [6] D. Prabakaran, Powerline communications—Electrifying the broadband [Online]. Available: <http://www.corridor.biz/pdf/PC-mag-article.pdf>.
- [7] H. Hrasnica, A. Haidine, and R. Lehnert, *Broadband Powerline Communications Networks: Network Design*. New York: Wiley, 2004.
- [8] R. M. van Maurick, "Potential common mode currents on the ISDN S and T-interface caused by cable unbalance," in *Proc. IEEE Int. Conf. Electromagnetic Compatibility*, 1992, no. 362, pp. 202–206.
- [9] C. R. Paul, *Analysis of Multiconductor Transmission Lines*. New York: Wiley, 1994.
- [10] S. Kim and D. P. Neikirk, "Compact equivalent circuit model for the skin effect," in *Proc. IEEE-MTT-S Int. Microwave Symp.*, R. G. Ranson, Ed., 1996, vol. 3, pp. 1815–1818.
- [11] D. K. Cheng, *Fundamental of Engineering Electromagnetics*. Reading, MA: Addison-Wesley, 1992.
- [12] K. Y. See, P. L. So, A. Kamarul, and E. Gunawan, "Radio-frequency common-mode noise propagation model for power-line cable," *IEEE Trans. Power Del.*, vol. 20, no. 4, pp. 2443–2449, Oct. 2005.

T. S. Pang received the B.Eng. degree in electrical and electronic engineering from Nanyang Technological University, Singapore, in 2004, where he is currently pursuing the Ph.D. degree.

His research interests are in the areas of power-line communications and electromagnetic-interference/electromagnetic-compatibility (EMI/EMC) design issues in power-line communication networks.

P. L. So (M'98–SM'03) received the B.Eng. degree (Hons.) in electrical engineering from the University of Warwick, Warwick, U.K., in 1993, and the Ph.D. degree in electrical power systems from Imperial College, University of London, London, U.K., in 1997.

Currently, he is an Associate Professor in the School of Electrical and Electronic Engineering, Nanyang Technological University, Singapore. He is also the Program Director (Power Line Communications) of the Network Technology Research Centre, Nanyang Technological University. Prior to his academic career, he was a Second Engineer with China Light and Power Co. Ltd., Hong Kong, China, in power system protection. His research interests are power system stability and control, flexible ac transmission systems (FACTS), power quality, and power-line communications.

Dr. So is Treasurer of the IEEE Singapore Section.

K. Y. See (SM'02) received the B.Eng. degree (Hons.) in electrical engineering from the National University of Singapore, in 1986 and the Ph.D. degree in electrical engineering from Imperial College, London, U.K., in 1997.

Currently, he is an Associate Professor in the School of Electrical and Electronic Engineering, Nanyang Technological University, Singapore. Prior to his academic career, he was Head of the Electromagnetic Compatibility (EMC) Centre, Singapore Technologies Electronic for five years, and another three years as Lead EMC Design Engineer with ASTEC Custom Power, Singapore. His research interests are computational electromagnetics, EMC design for power electronics, signal integrity issues for high-speed design, and EMC measurement techniques.

Dr. See is the Chair of the IEEE Singapore EMC Chapter, a Member of Singapore Technical Committee of EMC, and an active Laboratory Assessor of the Singapore Accreditation Council. He is also the Organizing Committee Chair of the 2006 EMC Zurich Symposium in Singapore.

A. Kamarul received the B.Eng. degree in electrical and electronic engineering from Nanyang Technological University, Singapore, in 2003 and is currently pursuing the M.Eng. degree from Nanyang Technological University.

From 2003 to 2004, he underwent a Research and Training Program in the area of optical communications with the Network Technology Research Center, Nanyang Technological University, under the sponsorship of the Economic Development Board of Singapore. His research interests are in power-line communications and electromagnetic-interference/electromagnetic-compatibility (EMI/EMC) design issues in power-line communication networks and systems.